Introduction

The pathophysiology of syringomyelia is still poorly understood. Many hypotheses exist in the literature[1–13], but they provide widely different explanations on the mechanisms of syrinx generation. There are, however, a few consensuses. First, the syrinx fluid is identical to the CSF, and there is some communication between the syrinx and the subarachnoid space. This point is supported by many studies[14–17]. Second, derangement of CSF flow in the spinal subarachnoid space is the main cause of syrinx generation both in Chiari-I malformation[7,18–21] and subarachnoid arachnopathy[22–25]. Notably, the cerebellar tonsil deranges the CSF flow in the former and adhesive arachnoiditis in the latter.

The problem, however, is where this communicating channel resides and what is the exact mechanism of syrinx generation. On these points, there is no solid experimental or clinical evidence, and the opinions of researchers vary widely. Gardner et al.[1] thought that the central canal intercommunicates the syrinx and the fourth ventricle, and pulsatile CSF pressure waves exerted on it generates the syrinx. Williams et al. also postulated the communication through the central canal, but he emphasized the craniospinal pressure gradient produced by Valsalva maneuver et al.[2].

On the other hand, Ball and Dayan[4] assumed that CSF entered the syrinx through the perivascular space of arteries penetrating the spinal cord. This idea has the following variations. Heiss et al.[7] proposed that the piston-like movement of the cerebellar tonsils in Chiari-I patients generated pressure waves in the spinal subarachnoid space. And it subsequently drove CSF into the syrinx through the perivascular space. Stoodley et al. also considered the perivascular space as the communicating channel, but he assumed the arterial pulse pressure as the driving force[26]. All these assumptions are not proven and remain hypothetical. Although recent researchers seem to favor the perivascular-space theory, there remains the possibility that a thin communicating channel exists between the syrinx and the fourth ventricle[27].

In our opinion, the main theoretical problems reside in the following points.

1. No theory can explain the pathophysiological mechanism of syringomyelia in a unified fashion.

2. No theory can explain how CSF enters from the low-pressure subarachnoid space to the high-pressure syrinx cavity and remains inside.

There are different types of syringomyelia such as Chiari-I-malformation and spinal-arachnopathy-related[22]. Also, the Chiari-I-malformation-related syringomyelia is further subdivided into communicating and non-communicating[28]. Despite the differences in etiology and imaging findings, the final phenomenon of syrinx formation is common among them. Therefore, we are tended to assume a common underlying mechanism in these different types of syringomyelia[26]. In fact, it is counter-intuitive to assume completely different mechanisms to these very similar pheomena, e.g. perivascular communication

for non-communicating syringomyelia, and central-canal communication for communicating syringomyelia.

The second point is theoretically essential but challenging to solve. Physical laws dictate that the expanded syrinx cavity has higher pressure than the adjacent subarachnoid space[7,29–31]. We can intuitively understand it by the fact that the inside pressure must additionally confront the elastic tension of the syrinx wall. Therefore, merely assuming a communicating channel does not explain how CSF enters and remains inside the syrinx against this pressure gradient. Even if we take a specific time window where the subarachnoid pressure exceeds the syrinx pressure, it does not explain how the CSF remains inside the syrinx after it. We will call this problem the pressure-gradient paradox in this article.

The current article is part of our effort to solve the above theoretical problems. We proposed in our previous paper[27] a hypothesis on the pathophysiology of syringomyelia as follows. Suppose, at a certain location in the spinal subarachnoid space, there exists a direction-selective resistance to CSF flow. For example, we can assume a resistance selectively resisting to the caudal flow and less resisting to the rostral flow. To-and-fro CSF movement across this resistance certainly affects the pressure inside the spinal cord matrix. We hypothesized that this repetitive pressure alteration inside the cord is related to the mechanism of syrinx generation. We would like to describe the detail of this theory in this article, which we could not elaborate in the previous article.

This hypothesis was attractive to us because it seemed to solve the two theoretical problems listed above. First, it could explain the two types of syringomyelia (Chiari-related and arachnopathy-related) in a unifying fashion. Namely, we could assume the tonsil and the adhesive arachnoid membrane both working as a direction-selective resistance. Second, this theory could solve the pressure-gradient paradox as will be seen below.

The analysis was carried out using our electric-circuit model of the spinal CSF dynamics, which we publised in our previous articles[11,12] and revised for the current purpose.

Material and Method

Our intention in this study was to make a basic model that could clarify the phenomenon underlying the syrinx generation and not to make a quantitatively precise model of the spinal CSF flow. There is a problem when we try to simulate the motion of biological fluids such as blood and CSF. Such bodily fluids move inside flexible tubes. It differs from the usual situation of fluid mechanics, where the boundary of the fluid conduit is solid. Thus, we cannot simply apply the standard Navier-Stokes equations for our simulation. For this reason, researchers have commonly used lumped parameter models[32,33]. This model interprets the fluid flow inside a flexible tube analogous to the electric flow in an electric circuit. The accumulation of electricity in a capacitor represents the expansion of a

flexible tube and the accompanying pressure elevation. An electrical resistor represents the frictional resistance to flow. Our current model is the type of lumped parameter model with multiple compartments[32,33] that simulates the CSF dynamics in the spine and is an updated version of the model used in our previous articles[11,12].

Figure 1 shows the scheme of our spinal CSF dynamics model. It included two CSF pathways along the spinal cord. One was the spinal subarachnoid space represented by the resistors designated with R. The other was an intraspinal pathway represented with resistors designated with r. This intraspinal pathway was envisaeged as the central canal, but could be any other CSF pathway postulated to be in the spinal cord. The rational for incorporating the central canal in the theory is thoroughly explained in our previous article[27]. The elasticity of the dura is represented by capacitors designated with D. The elasticity of the central canal is represented by capacitors designated with C. The elasticities at the major cistern and the lumbar theca are represented by C_{cist} and C_{thec}, respectively.

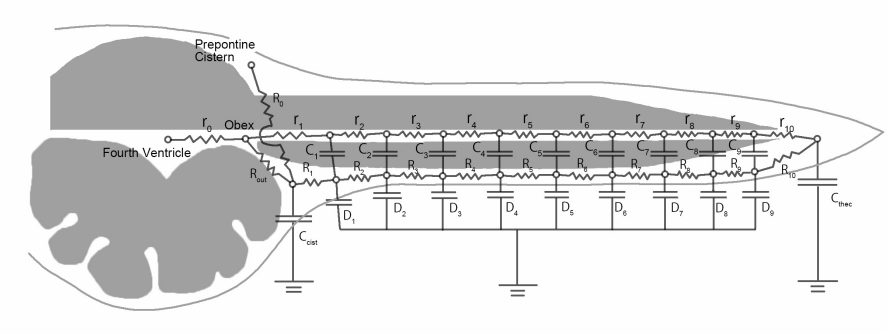

Figure 1: Schema of the electric circuit model of the CSF dynamics in the spine.

The concrete parameters were determined as follows.

- The number of nodes was 100.
- We set the length of the modeled spinal cord to be 1 meter.
- The resistance of the subarachnoid space (R) was estimated using the following equations of Poisseuille[34–36].

$$\Delta P = \frac{8\pi\mu LQ}{A^2} = RQ$$

  - ΔP: Pressure difference between the adjacent compartments
  - Q: flow speed per unit surface
  - μ: viscosity coefficient. In this case, it was set to the value of water (0.0007).

– L: distance between the adjacent compartments. It was set to 1 cm.

– A: cross sectional area of the subarachnoid space. It was set to the value of a concentric annulus[36] with the outer diameter of 1cm and the inner diameter of 0.7 cm ($1.6 \times 10^{-4}(m^2)$)

Thus, R was calculated to be 6872 $(Pa \cdot sec/m^3)$

- The resistance of the central canal (r) was estimated using the same equation with A set to $\pi(10^{-4})^2$ (m^2), i.e. the cross sectional area of a tube with a diameter of 100 μm. Thus, r was calculated to be 1.78×10^{11} $(Pa \cdot sec/m^3)$
- We determined the capacitance (C_{sub})corresponding to the dural elasticity so that the pressure-wave velocity determined by the time constant (RC) will roughly correspond to the pressure-wave velocity of the downward CSF wave observed in phase-contrast MRI of normal individuals. Thus, we set $C_{sub} = 0.1$ $(m^3/Pa \cdot sec)$.

Figure 2 shows the bare electric circuit extracted from Figure 1. A set of differential equations could describe the behavior of this model. Using computer software, we could numerically calculate its behavior in response to a certain cranial pressure wave (defined as a boundary condition on the cranial nodes). In our previous articles[11,12], we only analyzed the transient behavior of the model to a sudden pressure increase on the cranial side of the subarachnoid space. This analysis helped simulate the situation of coughing or Valsalva maneuvers. In this article, however, we analyzed the response of the model to an oscillating cranial pressure wave simulating the normal to-and-fro movement of the CSF.

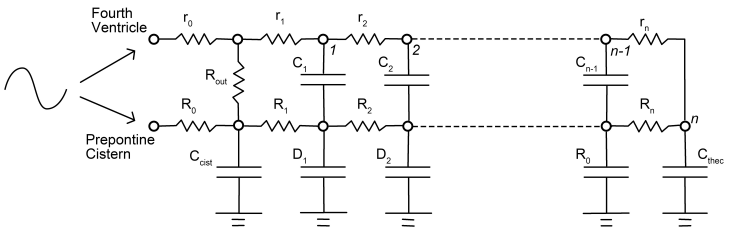

Figure 2: Electric circuit diagram representing the CSF dynamics of the spine

We described the differential equations on a computer software (Mathematica version 12, Wolfram Research, Champaign, IL, U.S.A.) and solved them numerically. We set the boundary conditions as follows. (1) The voltage at the two cranial nodes was set to a sine wave oscillating around 10 cmH_2O with an amplitude of 20 cmH_2O at one cycle per second. (2) The initial dural pressure was set at 10 cmH_2O in all segments. We set the step of the numerical solution to 1/5000 second and calculated the solution from zero to 20 seconds. The actual Mathematica codes can be found in our GitHub repository (https://github.com/chang-hs/syrinx_simulation.git).

We analyzed three different settings of the system. The first setting was the original normal system simulating the normal status. In the second setting, we simply increased the subarachnoid resistance at point 25 (R_{25}) by 20 times. In the third setting, we placed a direction-selective subarachnoid resistance at point 25, so that only the resistance to the caudal flow would be increased by 20 times.

Results

We present the systems' responses in animation. The x-axis of each animation represents the 100 nodes of the circuit laid out from the cranial to caudal direction. The y-axis displays a certain subset of the following four parameters: the dural tension (voltage in D capacitors in Figure 1, 2), the canal tension (voltages in C capacitors in Figure 1, 2), the subarachnoid CSF flow (flows in R resistors in Figure 1, 2), and the channel flow (flows in r resistors in Figure 1, 2). We plotted the caudal flow in the positive and the rostral flow in the negative direction. The pressure values are shown in cmH_2O, the flows in ml/sec. To plot the four parameters in a single animation, we multiplied the values of the following three parameters by certain coefficients. Namely, the canal tension was multiplied by 50, the subarachnoid flow by 0.005, and the canal flow by 1.5×10^5.

Video 1 shows the original system's response representing the normal condition. In this state, the dural tension made a smooth gradient along the spine, whose polarity alternated according to the pressure cycle. CSF made smooth to-and-fro movements in the subarachnoid space with the corresponding pressure wave along the dura and the central canal. CSF also made smooth to-and-fro movements in the intraspinal channel. Pressure elevation in the wall of the intra-spinal channel was minimal.

[movie] : totalAnimationNorm.mp4

In Video 2, we increased the subarachnoid resistance R_{25} by 20 times, thereby simulating a simple block of the subarachnoid flow in both directions. In this condition, both the caudal and rostral flow across the resistance produced pressure drop in the distal subarachnoid segment. This pressure drop caused an increase in canal flow in the same direction as the subarachnoid flow. This increased canal flow caused a transient increase in the canal pressure distal to

the block and a decrease proximal to the block. However, these pressure changes alternated along the alternation of the flow direction and did not produce a sustained pressure increase.

In Video 3, we replaced the subarachnoid resistor R_{25} with a direction-selective resistor whose resistance to the rostral flow was unchanged but that to the caudal flow was increased by 20 times. This time, sustained high pressure appeared in the intra-spinal channel in the segment distal to the replaced resistor, and sustained low pressure in the segment proximal to it. This sustained pressure gradually accumulated as the flow cycle proceeded. The dural tension showed a pressure drop at node 25 only during the caudal-flow phase. The to-and-fro canal flow increased near the node 25 similarly to that in the simple block above, but, this time, the increase was larger in the caudal direction.

We extracted the canal flow from this animation and showed it in Video 4. Observing this video, we can see that the cumulative total of the caudal flow is larger than that of the rostral flow, meaning that the CSF is virtually pumped caudally at node 25. To further elucidate this point, Video 4 simultaneously shows the canal flow in the simple block as shown in Video [video:simple_block] and that in the one-way block as shown in Video [video:oneway]. We can clearly see that the caudal flow is about the same in the two models, while the rostral flow is smaller in the direction-selective model. It means that CSF in the intra-spinal channel is pumped caudally in each cycle of the to-and-fro CSF movement.

Discussion

In this article, we theoretically analyzed the CSF movement in the spine using a lumped parameter model with multiple compartments. It simulated a system with an elastic tube (dura) containing an elastic cylindrical material (spinal cord) that itself had a fluid channel inside. When we placed a direction-selective resistor in the subarachnoid space and evoked a to-and-fro pressure wave on this system, it produced a sustained pressure elevation in the segment distal to the resistor in the resisted direction. This phenomenon may explain the pathogenesis of syringomyelia both in Chiari I malformation and syringomyelia associated with arachnopathy.

Subarachnoid pressure pushes the spinal cord material and affects the pressure inside the intra-spinal channel. As seen in Figure 2, the absolute pressure inside the intra-spinal channel is the sum of the subarachnoid and channel tension (voltages of C_k and D_k in electrical terms). Suppose a one-way valve selectively resists caudal flow in the subarachnoid space at point A. Caudal CSF flow creates a pressure drop across point A, with the caudal pressure smaller than the proximal one. Thus, the absolute pressure in the canal distal to point A become smaller because the outside subarachnoid pressure there is smaller. It, therefore, creates a pressure gradient in the central canal across point A, thereby increasing the distal CSF flow in the canal at that point (Figure 3).

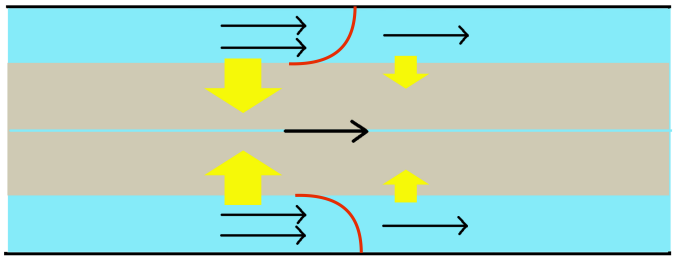

Figure 3: Increased central-canal flow across a direction-selective resistance in the subarachnoid space

On the contrary, rostral flow, not encountering resistance, does not create a pressure drop (Figure 4). Although some of the CSF that had been pumped caudally during the caudal-flow phase will flow back rostrally, its amount will be smaller. The net result will be that some CSF is pumped caudally in one cycle of the to-and-fro movement. Thus, CSF gradually accumulates in the distal segment of the resistance (Video 3). We hypothesize that this is the mechanism underlying the syrinx generation.

Our theory clearly explained how the CSF is paradoxically driven into the high-pressure syrinx and retained inside against the pressure gradient. In the direction-selective resistance model, the caudal segment of the intra-spinal channel has sustained higher pressure than the subarachnoid space. However, the energy of to-and-fro CSF movement creates alternating pressure gradient in the rostro-caudal direction. Because this rostro-caudal pressure gradient is larger than the sustained high pressure of the intra-spinal channel, CSF flows into the caudal segment from the rostral side during the caudal flow phase (Figurefig. 3). In the rostral flow phase, the rostro-caudal pressure gradient is reversed in direction; the pressure on the rostral side becomes smaller than that on the caudal side. CSF flows out rostrally from the caudal intra-spinal channel; however, because the pressure-drop effect caused by the subarachnoid resistance is absent in this phase, the rostro-caudal pressure gradient in the intra-spinal channel is smaller and the rostral CSF flow is smaller than that during the caudal flow phase (Figurefig. 4). We believe that this is the mechanism of the apparently paradoxical behavior of the CSF in syringomyelia.

Direction-selective resistance to CSF flow is not an imaginative assumption.

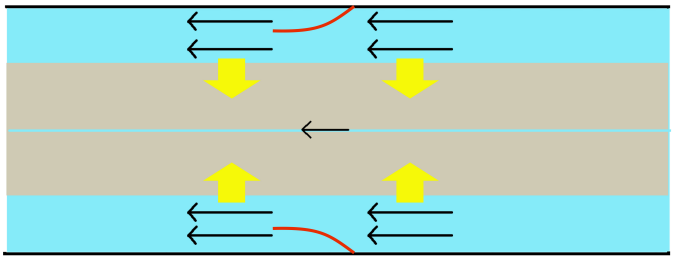

Figure 4: Normal central-canal flow across a direction-selective resistance during the reverse flow

In Chiari-I malformation, the herniated tonsils move like a ball-valve; they are displaced caudally during the caudal flow and rostrally during the rostral flow. The higher velocity observed in the phase-contrast MRI studies suggests that they selectively impede the caudal CSF flow more than the cranial flow. Williams et al. demonstrated direction-selective resistance at the craniovertebral junction of Chiari-I patients, which became the basis of his theory[37]. Also, some types of arachnoid pathology may function as one-way valves. In 2014, we reported cases of thoracic arachnoid web associated with syringomyelia, in which phase-contrast MRI demonstrated one-way-valve-like behavior of the arachnoid web[25]. In surgery, we found an obliquely oriented arachnoid web that resembled a one-way valve. Thus, our hypothesis may also solve the second theoretical problem we pointed out in the Introduction. Namely, the direction-selective resistance in spinal subarachnoid space may function as the common mechanism underlying both Chiari-I-related and arachnopathy-related syringomyelia.

transformed into the energy-requiring trasport of CSF into the syrinx. However, previous theories seemed to have difficulty in explaining this process. According to the theories of Heiss et al.[7] or that of Stoodley et al.[26], the energy is provided by either enhanced pressure waves in subarachnoid space or pulsation of spinal arteries. However, none of these theories explains the detailed mechanism

Our results may cast some light on another interesting question. In cervical spondylosis, subarachnoid space is similarly obliterated by the protruding discs and osteophytes. Although this is a widely prevaent disease, we rarely encounter syringomyelia associated with cervical spondylosis. In our results, a simple block of the subarachnoid CSF flow did not produce sustained elevation of intraspinal

channel pressure (Video 2). This result may explain why syringomyelia is rarely associated with cervical spondylosis.

There are some controversial points in our theory. Our model presumed the existence of a CSF channel inside the spinal cord. It may be controversial because most syringes seem to lack such communication. Yet, there still may exist a narrow CSF channel that is undetectable on MRI. In fact, ordinary MRI does not visualize the central canal with a diameter of 100 micrometers. Therefore, assuming the existence of a CSF channel inside the cord will not be far-fetched. Another point of controversy will be the role of the central canal. The human central canal is obstructed with advancing age, and assuming a function of the central canal may not befit that fact. However, the obliteration of the central canal seem to be a slow process, and it could be mostly patent up to the fourth decade[38,39]. Moreover, the CSF channel does not have to be the central canal but some other channel created inside the spinal cord matrix.

References

1. Gardner WJ, Angel J. The mechanism of syringomyelia and its surgical correction. *Clin Neurosurgery*. 1958;6:131-140.
2. Williams B. On the pathogenesis of syringomyelia: a review. *J R Soc Med*. 1980;73(11):798-806.
3. Milhorat TH, Chou MW, Trinidad EM, et al. Chiari I malformation redefined: clinical and radiographic findings for 364 symptomatic patients. *Neurosurgery*. 1999;44(5):1005-1017. doi:10.1097/00006123-199905000-00042
4. Ball MJ, Dayan AD. Pathogenesis of syringomyelia. *Lancet*. 1972;2(7781):799-801. doi:10.1016/s0140-6736(72)92152-6
5. Klekamp J. The pathophysiology of syringomyelia - historical overview and current concept. *Acta Neurochir (Wien)*. 2002;144(7):649-664. doi:10.1007/s00701-002-0944-3
6. du Boulay G, Shah SH, Currie JC, Logue V. The mechanism of hydromyelia in Chiari type 1 malformations. *Br J Radiol*. 1974;47(561):579-587. doi:10.1259/0007-1285-47-561-579
7. Heiss JD, Patronas N, DeVroom HL, et al. Elucidating the pathophysiology of syringomyelia. *J Neurosurg*. 1999;91(4):553-562. doi:10.3171/jns.1999.91.4.0553
8. Milhorat TH, Miller JI, Johnson WD, Adler DE, Heger IM. Anatomical basis of syringomyelia occurring with hindbrain lesions. *Neurosurgery*. 1993;32(5):748-754; discussion 754. doi:10.1227/00006123-199305000-00008
9. Stoodley MA. Pathophysiology of syringomyelia. *J Neurosurg*. 2000;92(6):1069-1070; author reply 1071-1073.

10. Terae S, Miyasaka K, Abe S, Abe H, Tashiro K. Increased pulsatile movement of the hindbrain in syringomyelia associated with the Chiari malformation: cine-MRI with presaturation bolus tracking. *Neuroradiology*. 1994;36(2):125-129.

11. Chang HS, Nakagawa H. Hypothesis on the pathophysiology of syringomyelia based on simulation of cerebrospinal fluid dynamics. *J Neurol Neurosurg Psychiatr*. 2003;74(3):344-347.

12. Chang HS, Nakagawa H. Theoretical analysis of the pathophysiology of syringomyelia associated with adhesive arachnoiditis. *J Neurol Neurosurg Psychiatr*. 2004;75(5):754-757.

13. Greitz D. Unraveling the riddle of syringomyelia. *Neurosurg Rev*. 2006;29(4):251-263; discussion 264. doi:10.1007/s10143-006-0029-5

14. Ellertsson AB. Syringomyelia and other cystic spinal cord lesions. *Acta Neurol Scand*. 1969;45(4):403-417. doi:10.1111/j.1600-0404.1969.tb01254.x

15. Ellertsson AB, Greitz T. Myelocystographic and fluorescein studies to demonstrate communication between intramedullary cysts and the cerebrospinal fluid space. *Acta Neurol Scand*. 1969;45(4):418-430.

16. Li KC, Chui MC. Conventional and CT metrizamide myelography in Arnold-Chiari I malformation and syringomyelia. *AJNR Am J Neuroradiol*. 1987;8(1):11-17.

17. Heiss JD, Jarvis K, Smith RK, et al. Origin of Syrinx Fluid in Syringomyelia: A Physiological Study. *Neurosurgery*. 2019;84(2):457-468. doi:10.1093/neuros/nyy072

18. Wolpert SM, Bhadelia RA, Bogdan AR, Cohen AR. Chiari I malformations: assessment with phase-contrast velocity MR. *AJNR Am J Neuroradiol*. 1994;15(7):1299-1308.

19. Bhadelia RA, Bogdan AR, Wolpert SM, Lev S, Appignani BA, Heilman CB. Cerebrospinal fluid flow waveforms: analysis in patients with Chiari I malformation by means of gated phase-contrast MR imaging velocity measurements. *Radiology*. 1995;196(1):195-202. doi:10.1148/radiology.196.1.7784567

20. Hofmann E, Warmuth-Metz M, Bendszus M, Solymosi L. Phase-contrast MR imaging of the cervical CSF and spinal cord: volumetric motion analysis in patients with Chiari I malformation. *AJNR Am J Neuroradiol*. 2000;21(1):151-158.

21. Quigley MF, Iskandar B, Quigley ME, Nicosia M, Haughton V. Cerebrospinal fluid flow in foramen magnum: temporal and spatial patterns at MR imaging in volunteers and in patients with Chiari I malformation. *Radiology*. 2004;232(1):229-236. doi:10.1148/radiol.2321030666

22. Klekamp J, Batzdorf U, Samii M, Bothe HW. Treatment of syringomyelia associated with arachnoid scarring caused by arachnoiditis or trauma. *J Neurosurg.* 1997;86(2):233-240. doi:10.3171/jns.1997.86.2.0233

23. Brodbelt AR, Stoodley MA, Watling AM, Tu J, Burke S, Jones NR. Altered subarachnoid space compliance and fluid flow in an animal model of posttraumatic syringomyelia. *Spine.* 2003;28(20):E413-419. doi:10.1097/01.BRS.0000092346.83686.B9

24. Heiss JD, Snyder K, Peterson MM, et al. Pathophysiology of primary spinal syringomyelia. *J Neurosurg Spine.* 2012;17(5):367-380. doi:10.3171/2012.8.SPINE111059

25. Chang HS, Nagai A, Oya S, Matsui T. Dorsal spinal arachnoid web diagnosed with the quantitative measurement of cerebrospinal fluid flow on magnetic resonance imaging. *J Neurosurg Spine.* 2014;20(2):227-233. doi:10.3171/2013.10.SPINE13395

26. Stoodley MA, Jones NR, Yang L, Brown CJ. Mechanisms underlying the formation and enlargement of noncommunicating syringomyelia: experimental studies. *Neurosurgical Focus.* 2000;8(3):1-7. doi:10.3171/foc.2000.8.3.2

27. Chang HS. *Hypothesis on the Pathophysiology of Syringomyelia Based on Analysis of Phase-Contrast Magnetic Resonance Imaging of Chiari-I Malformation Patients.* F1000Research; 2021. doi:10.12688/f1000research.72823.1

28. Elliott NSJ, Bertram CD, Martin BA, Brodbelt AR. Syringomyelia: A review of the biomechanics. *Journal of Fluids and Structures.* 2013;40:1-24. doi:10.1016/j.jfluidstructs.2013.01.010

29. Serway, R. A. Fluids and Solids. In: *College Physics.* 11th ed. Cengage Learning; 2016:267-319.

30. Davis CH, Symon L. Mechanisms and treatment in posttraumatic syringomyelia. *Br J Neurosurg.* 1989;3(6):669-674. doi:10.3109/02688698908992690

31. Ellertsson AB, Greitz T. The distending force in the production of communicating syringomyelia. *Lancet.* 1970;1(7658):1234. doi:10.1016/s0140-6736(70)91829-5

32. Shi Y, Lawford P, Hose R. Review of Zero-D and 1-D Models of Blood Flow in the Cardiovascular System. *BioMed Eng OnLine.* 2011;10(1):33. doi:10.1186/1475-925X-10-33

33. Kokalari I, Karaja T, Guerrisi M. Review on lumped parameter method for modeling the blood flow in systemic arteries. *J Biomed Sci Eng.* 2013;6(1):92-99.

34. Brook BS, Falle S, Pedley TJ. Numerical solutions for unsteady gravity-driven flows in collapsible tubes: evolution and roll-wave instability of a steady state. *Journal of Fluid Mechanics.* 1999;396:223-256.

35. Sherwin SJ, Formaggia L, Peiro J, Franke V. Computational modelling of 1D blood flow with variable mechanical properties and its application to the simulation of wave propagation in the human arterial system. *International journal for numerical methods in fluids*. 2003;43(6-7):673-700.

36. Huilgol RR, Georgiou GC. A fast numerical scheme for the Poiseuille flow in a concentric annulus. *Journal of Non-Newtonian Fluid Mechanics*. 2020;285:104401. doi:10.1016/j.jnnfm.2020.104401

37. Williams B. Simultaneous cerebral and spinal fluid pressure recordings. 2. Cerebrospinal dissociation with lesions at the foramen magnum. *Acta Neurochir (Wien)*. 1981;59(1-2):123-142. doi:10.1007/BF01411198

38. Newman PK, Terenty TR, Foster JB. Some observations on the pathogenesis of syringomyelia. *J Neurol Neurosurg Psychiatry*. 1981;44(11):964-969. doi:10.1136/jnnp.44.11.964

39. Yasui K, Hashizume Y, Yoshida M, Kameyama T, Sobue G. Age-related morphologic changes of the central canal of the human spinal cord. *Acta Neuropathol*. 1999;97(3):253-259.